

Research Paper

Pulsatile Powell-Eyring Nanofluid Flow in a Channel with Inclined Magnetic Field and Chemical Reaction

Suripeddi SRINIVAS¹), Kalyan Kumar CHALLA²)*,
Satyanarayana BADETI¹), P. Bharath KUMAR¹)

¹) *Department of Mathematics, School of Advanced Sciences, VIT-AP University*
Inavolu, Vijayawada-522237, India

²) *Department of Mathematics, Narayana Engineering College (Autonomous)*
Gudur, Tirupati-524 101, India

*Corresponding Author e-mail: kalyankumar.challa@gmail.com

The current article addresses the impacts of the pulsatile flow of Powell-Eyring nanofluid using Buongiorno's model in a horizontal channel. It also describes the combined impacts of thermophoresis and Brownian motion. Blood is an example of a Powell-Eyring fluid. The Runge-Kutta (R-K) 4th-order method, along with the shooting technique, is used to determine solutions for velocity, temperature, and concentration. The impacts of different parameters, including an inclined magnetic field, chemical reaction, Lewis number, and heat source or sink parameter, are illustrated graphically. The mass flux distribution decreases due to an increase in the values of the Powell-Eyring fluid parameter.

Keywords: Powell-Eyring nanofluid; inclined magnetic field; chemical reaction; pulsatile flow; mass flux.

1. INTRODUCTION

Nanofluids are different types of fluid composed of convectational base liquids and nanometre-sized particles. Nanofluid research is a significant scientific field because of its wide range of potential applications in mineral oil, water, solar energy, and microelectronics. In chemotherapy, nanoparticles are also utilised to kill cancer cells. Applications of nanofluids in technology and engineering include cancer therapeutics, vehicle thermal management, nuclear systems cooling, intensified microreactors, electronic cooling components, and many more. Several studies on these fluids are cited in [1–3]. The entropy generation in hydromagnetic Powell-Eyring nanofluid flow was studied by ALSAEDI *et al.* [4]. BUONGIORNO [5] examined the convective heat transport in nanofluids. In this study, the author developed a two-component, four-equation nonhomogeneous

equilibrium model for mass momentum and heat transport in nanofluids. Furthermore, BUONGIORNO [5] concluded that in the absence of turbulent effects, Brownian diffusion and thermophoresis would be important. In addition, he has considered the conservation equations based on these two effects. HAYAT *et al.* [6] provided an explanation for an Eyring-Powell nanofluid across a non-linear stretching surface. In a vertical channel, pulsatile Casson nanofluid flow was examined by KUMAR *et al.* [7] using Buongiorno's model. MALLICK and MISRA [8] described how an electromagnetic field affects the peristaltic flow of a Powell-Eyring nanofluid in an asymmetric wavy microchannel. In an L-shaped enclosure, nanofluid free convection heat transfer was demonstrated by SHEIKH-HOLESLAMI *et al.* [9]. The impacts of convective heat transport of nanofluid in a wavy channel were analytically examined by SHEHZAD *et al.* [10].

Magnetohydrodynamics (MHD) flow has been the subject of numerous theoretical and empirical studies across various physical, geophysical, and industrial fields. The applications of MHD flows are found in a wide range of industrial domains, such as electronic packages, microelectronic devices, cooling of nuclear reactors, crystal growth in liquids, and electric propulsion for space exploration. An inclined magnetic field has a non-zero inclination angle. Significant advancements in the study of inclined magnetic field flow with heat transfer were made in [11–15]. KALADHAR *et al.* [16] explained the influences of the Hall current, thermal radiation, and an inclined magnetic field on fully developed electrically conducting mixed convection flow between vertical parallel plates. NATH and MURUGESAN [17] explored the formation of a nanoparticle that affects mass and heat transport processes in a moving lid cavity with an inclined magnetic field. The flow of viscous liquid inclined magnetic field with peristalsis was studied by NOREEN and QASIM [18].

There have been numerous studies on pulsatory flows in channels and pipes [19–24]. However, very few studies on non-Newtonian nanofluid flow with pulsating pressure gradients have been documented in the literature. DATTA *et al.* [25] explored the dusty liquid flow in a channel. The effect of pulsatile blood flow in thermally significant blood vessels on the thermal lesion region during thermal therapy of tumor was studied by HORNG *et al.* [26]. KUMAR and SRINIVAS [27] examined pulsating Casson fluid flow in a vertical channel. The effects of pulsatility, catheterization, the non-Newtonian nature of blood and peripheral layer thickness on various flow quantities were analyzed by SANKAR [28]. The oscillatory flow of dusty MHD Ree-Eyring fluid with heat transfer in a channel was discussed by SHAWKY [29]. SRINIVAS *et al.* [30] investigated the cross-diffusion effects of pulsating Casson fluid flow in a vertical permeable channel. THAMIZHARASAN and REDDY [31] examined MHD Jeffrey nanofluid with pulsation, in a channel. Very recently, WANG *et al.* [32] studied pulsatory blood flow pass a small vessel under a magnetic field.

The primary goal of this work is to conduct the numerical analysis of hydro-magnetic Powell-Eyring nanofluid flow between two parallel walls generated by a pulsating pressure gradient. To study how to regulate the motion of the fluid by altering these characteristics and external forces, it is necessary to demonstrate the relationship between the various motion parameters and external forces. The article is structured as follows. The modelling and formulation of the problem are presented in Sec. 2. The problem’s solution is presented in Sec. 3. In Sec. 4, discussions are presented with the aid of graphs and tables. Finally, Sec. 5 provides a summary of the key findings.

2. MODELLING AND FORMULATION

Consider a fully developed laminar pulsatory flow of an electrically conducting Powell-Eyring nanofluid between two parallel walls separated by a distance h . A uniform strength magnetic field B_0 is applied at an inclined location of angle α with respect to the x^* -axis (see Fig. 1). The fluid velocity, temperature and concentration are assumed to be parallel to the x^* -axes. So that only the x^* -component of u^* velocity does not vanish. The condition of fully developed flow implies that $\frac{\partial u^*}{\partial x^*} = 0$. Given the velocity is solenoidal, we obtain $\frac{\partial v^*}{\partial y^*} = 0$. As a consequence, the velocity component v^* is constant in any channel section and is equal to zero at the channel walls, indicating that v^* must be vanishing at any position. The y^* -momentum balance equation can be expressed as $\frac{\partial p^*}{\partial y^*} = 0$. Here T_0, C_0 represents the temperature and concentration at the lower wall, while the uniform temperature and concentration, T_1, C_1 , are considered on the upper wall. The flow of the fluid in the channel is influenced by a pulsatory pressure gradient (THAMIZHARASAN and REDDY [31]):

$$(2.1) \quad -\frac{1}{\rho_f} \frac{\partial P^*}{\partial x^*} = A_0 \left(1 + \varepsilon e^{i\omega t^*} \right), \quad \varepsilon \ll 1,$$

where ε is a suitably chosen positive quantity (RADHAKRISHNAMACHARYA and MAITI [22] and SANKAR [28]), A_0 is a known constant, t^* is time, P^* is the di-

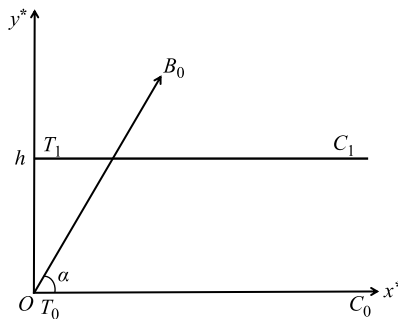


FIG. 1. Flow domain schematic diagram.

mensional pressure, and ω is the frequency. The rheological equation of the non-Newtonian Eyring-Powell-Cauchy model is defined by MALLICK and MISRA [8] as

$$S_{ij} = \mu_f \frac{\partial u_i^*}{\partial x_j^*} + \frac{1}{\beta} \sinh^{-1} \left(\frac{1}{L} \frac{\partial u_i^*}{\partial x_j^*} \right),$$

where β and L are fluid material constants, u_i^* represents velocity, S_{ij} is the Cauchy tensor, and μ_f stands for dynamic viscosity. Since $\sinh^{-1} x \approx x$ of $|x| \leq 1$, then

$$S_{ij} = \mu_f \frac{\partial u_i^*}{\partial x_j^*} + \frac{1}{\beta} \left(\frac{1}{L} \frac{\partial u_i^*}{\partial x_j^*} \right) = \mu_f \left(1 + \frac{1}{\beta L \mu_f} \right) \frac{\partial u_i^*}{\partial x_j^*}.$$

The governing equations are [24, 31]:

$$(2.2) \quad \frac{\partial u^*}{\partial t^*} = -\frac{1}{\rho_f} \frac{\partial P^*}{\partial x^*} + \nu_f \left(1 + \frac{1}{\beta L \mu_f} \right) \frac{\partial^2 u^*}{\partial y^{*2}} - \frac{\sigma_f B_0^2}{\rho_f} u^* \sin^2 \alpha,$$

$$(2.3) \quad \frac{\partial T^*}{\partial t^*} = \frac{\kappa_f}{(\rho C_p)_f} \frac{\partial^2 T^*}{\partial y^{*2}} + \tau \left[D_B \left(\frac{\partial C^*}{\partial y^*} \frac{\partial T^*}{\partial y^*} \right) + \frac{D_T}{T_m} \left(\frac{\partial T^*}{\partial y^*} \right)^2 \right] \\ + \frac{\mu_f}{(\rho C_p)_f} \left(1 + \frac{1}{\beta L \mu_f} \right) \left(\frac{\partial u^*}{\partial y^*} \right)^2 - \frac{1}{(\rho C_p)_f} \frac{\partial q_r}{\partial y^*} + \frac{Q_0}{(\rho C_p)_f} (T^* - T_0),$$

$$(2.4) \quad \frac{\partial C^*}{\partial t^*} = D_B \frac{\partial^2 C^*}{\partial y^{*2}} + \frac{D_T}{T_m} \frac{\partial^2 T^*}{\partial y^{*2}} - k_1 C^*.$$

Subject to the boundary conditions:

$$(2.5) \quad \begin{aligned} u^*(0) &= 0, & T^*(0) &= T_0, & C^*(0) &= C_0, \\ u^*(h) &= 0, & T^*(h) &= T_1, & C^*(h) &= C_1, \end{aligned}$$

where $\tau = (\rho C_p)_p / (\rho C_p)_f$, $(\rho C_p)_p$ is the effective heat capacity of the nanoparticles, $(\rho C_p)_f$ is the heat capacitance of nanofluid, ρ_f is the density of the base fluid, ρ_p is the density of the particles, D_T is thermophoretic diffusion coefficient, ν_f is the kinematic viscosity, σ_f is electrical conductivity, D_B is the Brownian diffusion coefficient, T^* , C^* represents the dimensional temperature and concentration of the fluid, respectively, T_m is the mean temperature, κ_f is the thermal conductivity, Q_0 indicates the heat source (or sink), and k_1 is 1st-order chemical reaction rate. By using the Rosseland approximation for radiative heat flux, q_r is defined as

$$(2.6) \quad q_r = -\frac{4}{3} \left(\frac{\partial T^{*4}}{\partial y^*} \right) \frac{\sigma^*}{\chi},$$

where σ^* is the Stefan-Boltzmann constant, and χ is the Rosseland mean absorption co-efficient. We assume that the temperature differences within the flow are sufficiently small such that T^{*4} may be expressed as a linear function of the temperature. This is accomplished by expanding T^{*4} in a Taylor series about T_0 and neglecting higher-order terms, thus: $T^{*4} \cong 4T_0^3T^* - 3T_0^4$.

Therefore, Eq. (2.3) becomes

$$(2.7) \quad \frac{\partial T^*}{\partial t^*} = \frac{1}{(\rho C_p)_f} \left(\kappa_f + \frac{16\sigma^* T_0^3}{3\chi} \right) \frac{\partial^2 T^*}{\partial y^{*2}} + \tau \left[D_B \left(\frac{\partial C^*}{\partial y^*} \frac{\partial T^*}{\partial y^*} \right) + \frac{D_T}{T_m} \left(\frac{\partial T^*}{\partial y^*} \right)^2 \right] + \frac{\mu_f}{(\rho C_p)_f} \left(1 + \frac{1}{\beta L \mu_f} \right) \left(\frac{\partial u^*}{\partial y^*} \right)^2 + \frac{Q_0}{(\rho C_p)_f} (T^* - T_0).$$

We introduce non-dimensional variables:

$$(2.8) \quad \begin{aligned} P^* &= PA_0 \rho_f h, & t^* &= \frac{t}{\omega}, & T^* &= T_0 + \theta(T_1 - T_0), \\ u^* &= \frac{A_0}{\omega} u, & y^* &= yh, & x^* &= xh, & C^* &= C_0 + \phi(C_1 - C_0), \end{aligned}$$

where ω is the frequency, u, θ, ϕ represents the velocity, temperature, and concentration in dimensionless form, respectively. Transforming Eqs. (2.1), (2.2), (2.7), and (2.4) by using Eq. (2.8), we obtain

$$(2.9) \quad -\frac{\partial P}{\partial x} = 1 + \varepsilon e^{it},$$

$$(2.10) \quad \frac{\partial u}{\partial t} = -\frac{\partial P}{\partial x} + \frac{1+k_0}{H^2} \left(\frac{\partial^2 u}{\partial y^2} \right) - \frac{M^2}{H^2} \sin^2 \alpha u,$$

$$(2.11) \quad \begin{aligned} \frac{\partial \theta}{\partial t} &= \frac{1}{\text{Pr} H^2} \left(1 + \frac{4}{3} \text{Rd} \right) \frac{\partial^2 \theta}{\partial y^2} + \frac{1+k_0}{H^2} \text{Ec} \left(\frac{\partial u}{\partial y} \right)^2 \\ &\quad + \frac{\text{Nb}}{H^2} \frac{\partial \theta}{\partial y} \frac{\partial \phi}{\partial y} + \frac{\text{Nt}}{H^2} \left(\frac{\partial \theta}{\partial y} \right)^2 + \frac{Q}{H^2} \theta, \end{aligned}$$

$$(2.12) \quad \frac{\partial \phi}{\partial t} = \frac{1}{\text{Le Pr} H^2} \frac{\partial^2 \phi}{\partial y^2} + \frac{1}{\text{Le Pr} H^2} \frac{\text{Nt}}{\text{Nb}} \frac{\partial^2 \theta}{\partial y^2} - \frac{\gamma}{H^2} \phi - \frac{K_1}{H^2},$$

where $k_0 = \frac{1}{\beta L \mu_f}$ (Powell-Eyring fluid parameter), $M = \frac{B_0 h \sqrt{\sigma_f}}{\sqrt{\mu_f}}$ (Hartmann number), $H = \frac{h \sqrt{\omega}}{\sqrt{\nu_f}}$ (frequency parameter), $\text{Pr} = \frac{\mu C_p}{\kappa_f}$ (Prandtl number), $Q = \frac{Q_0 h^2}{(\rho C_p)_f \nu_f}$ (heat source/sink parameter), $\text{Nt} = \frac{\tau D_T (T_1 - T_0)}{T_m \nu_f}$ (thermophoresis

parameter), $\text{Ec} = \frac{(\frac{A_0}{\omega})^2}{C_p(T_1 - T_0)}$ (Eckert number), $\text{Rd} = \frac{4\sigma^* T_0^3}{\kappa_f \chi}$ (radiation parameter), $\text{Nb} = \frac{\tau D_B (C_1 - C_0)}{\nu_f}$ (Brownian motion parameter), $\gamma = \frac{k_1 h^2}{\nu_f}$ (chemical reaction parameter), $K_1 = \frac{k_1 C_0 h^2}{\nu_f (C_1 - C_0)}$, $\text{Le} = \frac{\alpha_0}{D_B}$ (Lewis number), and $\alpha_0 = \frac{\kappa_f}{(\rho C_p)_f}$ (thermal diffusivity).

The transformed boundary conditions (2.5) are

$$(2.13) \quad \begin{aligned} u(0) &= 0, & \theta(0) &= 0, & \phi(0) &= 0; \\ u(1) &= 0, & \theta(1) &= 1, & \phi(1) &= 1. \end{aligned}$$

3. METHOD OF SOLUTION

To obtain the solution of Eqs. (2.10)–(2.12), a perturbative solution was assumed in the form:

$$(3.1) \quad u = u_0 + \varepsilon u_1 e^{it} + \varepsilon^2 u_2 e^{2it},$$

$$(3.2) \quad \theta = \theta_0 + \varepsilon \theta_1 e^{it} + \varepsilon^2 \theta_2 e^{2it},$$

$$(3.3) \quad \phi = \phi_0 + \varepsilon \phi_1 e^{it} + \varepsilon^2 \phi_2 e^{2it},$$

while neglecting higher orders. Here, $\phi_1(y)$ and $\phi_2(y)$ are unsteady concentration profiles, $\theta_1(y)$ and $\theta_2(y)$ are unsteady temperature profiles, $u_1(y)$ and $u_2(y)$ are unsteady velocity profiles, $\phi_0(y)$ is the steady concentration profile, $\theta_0(y)$ is the steady temperature profile, $u_0(y)$ is the steady velocity profile, and u is the non-dimensional velocity.

Substituting Eqs. (2.9), (3.1)–(3.3) into Eqs. (2.10)–(2.12) and comparing the coefficients of the same powers of ε , we obtain:

$$(3.4) \quad (1 + k_0) u_0'' - M^2 \sin^2 \alpha u_0 + H^2 = 0,$$

$$(3.5) \quad (1 + k_0) u_1'' - (M^2 \sin^2 \alpha + iH^2) u_1 + H^2 = 0,$$

$$(3.6) \quad (1 + k_0) u_2'' - (M^2 \sin^2 \alpha + 2iH^2) u_2 = 0,$$

$$(3.7) \quad \left(1 + \frac{4}{3} \text{Rd}\right) \theta_0'' + (1 + k_0) \text{Pr Ec} (u_0')^2 + \text{Pr Nb} \theta_0' \phi_0' \\ + \text{Pr Nt} (\theta_0')^2 + \text{Pr Q} \theta_0 = 0,$$

$$(3.8) \quad \left(1 + \frac{4}{3} \text{Rd}\right) \theta_1'' + (\text{Pr} Q - i \text{Pr} H^2) \theta_1 + 2(1 + k_0) \text{Pr Ec} u_0' u_1' + \text{Pr Nb} (\theta_0' \phi_1' + \theta_1' \phi_0') + 2 \text{Pr Nt} \theta_0' \theta_1' = 0,$$

$$(3.9) \quad \left(1 + \frac{4}{3} \text{Rd}\right) \theta_2'' + (\text{Pr} Q - 2i \text{Pr} H^2) \theta_2 + (1 + k_0) \text{Pr Ec} ((u_1')^2 + 2u_0' u_2') + \text{Pr Nb} (\theta_0' \phi_2' + \theta_1' \phi_1' + \theta_2' \phi_0') + \text{Pr Nt} ((\theta_1')^2 + 2\theta_0' \theta_2') = 0,$$

$$(3.10) \quad \phi_0'' - \gamma \text{Pr Le} \phi_0 + \left(\frac{\text{Nt}}{\text{Nb}}\right) \theta_0'' - K_1 \text{Pr Le} = 0,$$

$$(3.11) \quad \phi_1'' - \text{Pr Le} (\gamma + iH^2) \phi_1 + \left(\frac{\text{Nt}}{\text{Nb}}\right) \theta_1'' = 0,$$

$$(3.12) \quad \phi_2'' - \text{Pr Le} (\gamma + 2iH^2) \phi_2 + \left(\frac{\text{Nt}}{\text{Nb}}\right) \theta_2'' = 0.$$

The corresponding boundary conditions are:

$$(3.13) \quad \begin{aligned} u_2(0) &= 0, & u_1(0) &= 0, & u_0(0) &= 0, \\ u_2(1) &= 0, & u_1(1) &= 0, & u_0(1) &= 0; \\ \theta_2(0) &= 0, & \theta_1(0) &= 0, & \theta_0(0) &= 0, \\ \theta_2(1) &= 0, & \theta_1(1) &= 0, & \theta_0(1) &= 1; \\ \phi_2(0) &= 0, & \phi_1(0) &= 0, & \phi_0(0) &= 0, \\ \phi_2(1) &= 0, & \phi_1(1) &= 0, & \phi_0(1) &= 1. \end{aligned}$$

By solving Eqs. (3.4)–(3.6) with the corresponding boundary conditions (3.13), one obtains:

$$(3.14) \quad u_0 = A_1 e^{m_1 y} + A_2 e^{m_2 y} + A_3,$$

$$(3.15) \quad u_1 = A_4 e^{m_3 y} + A_5 e^{m_4 y} + A_6,$$

$$(3.16) \quad u_2 = A_7 e^{m_5 y} + A_8 e^{m_6 y},$$

where m 's and A 's are constants given in the Appendix.

Further more, the non-dimensional mass flux (Q_1), rate of mass transfer (Sh), and heat transfer rate (Nu) at the channel boundaries can be obtained from:

$$(3.17) \quad Q_1 = \int_0^1 u \, dy, \quad \text{Nu} = -\frac{\partial \theta}{\partial y} \Big|_{y=0,1}, \quad \text{and} \quad \text{Sh} = -\frac{\partial \phi}{\partial y} \Big|_{y=0,1}.$$

4. RESULTS AND DISCUSSION

The system of dimensionless coupled ODEs (3.4)–(3.12), subject to the boundary conditions in Eq. (3.13), is numerically solved by employing the fourth-order Runge-Kutta scheme together with the shooting method using the NDSolve function in Mathematica, which is a current specialized computing system. NDSolve gives the solutions iteratively. The shooting technique is used via NDSolve. This technique is very helpful in the case of small step sizes featuring a negligible error. The step size is fixed as 0.001 (i.e., $\Delta y = 0.001$), maintaining constant precision for the convergence standards. Throughout the calculations, the employed parametric values are $Nt = 0.2$, $Le = 1$, $\gamma = 1$, $K_1 = 0.001$, $Nb = 0.2$, $Pr = 21$, $H = 2$, $Q = -2$, $Ec = 0.5$, $k_0 = 1.2$, $Rd = 2$, $\alpha = \pi/6$, $M = 2$, $t = \pi/4$, and $\varepsilon = 0.01$. Figure 2 depicts the changes in the velocity distribution for various parameters of k_0 , M , H , and α .

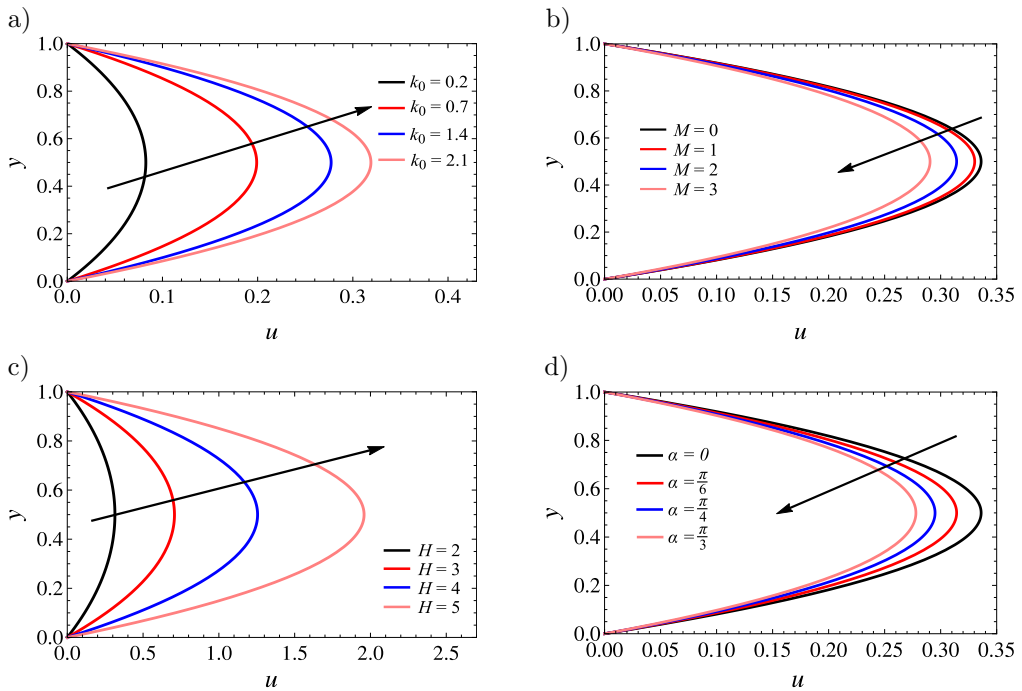


FIG. 2. Velocity distributions; impacts of: a) k_0 , b) M , c) H , d) α .

Figure 2a shows variation in velocity profile for different values of k_0 . An ascending trend in velocity profiles is observed for increasing values of k_0 , and this increases the thickness of the momentum boundary layer. Since k_0 is inversely proportional to the base fluid viscosity, increase in positive values of k_0 decreases the base fluid viscosity and enhances the stress rate within the boundary layer.

With a rise in k_0 , it is seen that the distributions of velocity increase. Figure 2b elucidates the effect of M on the velocity field. The applied magnetic field produces a drag force opposing the flow direction. As a result, the fluid’s velocity decreases with increasing magnetic field strength. Figure 2c reveals that velocity is increased for higher values of the frequency parameter (H).

The effect of the angle of inclination on u is plotted in Fig. 2d. It is evident that increasing values of α result in a decrease in u . This is because when α increases, the impact of the magnetic field on fluid particles rises, increasing the retarding force. As a result, the velocity field diminishes. The unsteady velocity distribution concerning the frequency parameter H and time t values are displayed in Fig. 3. Unsteady velocity profiles in Fig. 3a display fluctuating characteristics with an increasing frequency parameter H . The profiles are nearly parabolic in shape for small value of H . The highest velocity is observed near the boundary layers close to the walls. One can see in Fig. 3b that the unstable velocity distributions oscillate as t increases.

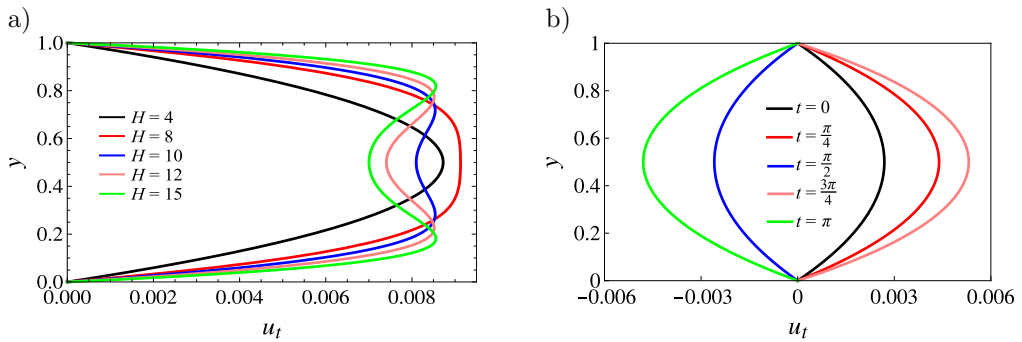


FIG. 3. Unsteady velocity distributions; impacts of: a) H , b) t .

Figure 4 illustrates the impacts of Nb , Nt , Ec , and Q on θ . Figure 4a depicts the variations in temperature distribution with changes in Nb . It is obvious that increasing Nb will significantly rise the fluid’s temperature. By changing Nt on θ , similar behaviour can be observed (see Fig. 4b). A rise in the Eckert number shows a high kinetic energy, which causes fluid molecules to vibrate and collide more frequently. Consequently, higher temperature profile (Fig. 4c) result from enhanced heat dissipation in the boundary layer region due to increased molecular collisions. Figure 4d illustrates how Q affects changes in the Powell-Eyring nanofluid’s temperature. The temperature of the fluid rises with the increase of heat source parameter, which results from the fluid’s heat generation. At the same time, quite the opposite behaviour can be observed for the increasing values of the ($Q < 0$) resulting from the fluid’s heat absorption. The influences of Nb , Nt , Ec , and t on θ_t are shown in Fig. 5. Figures 5a–5c describe the variation

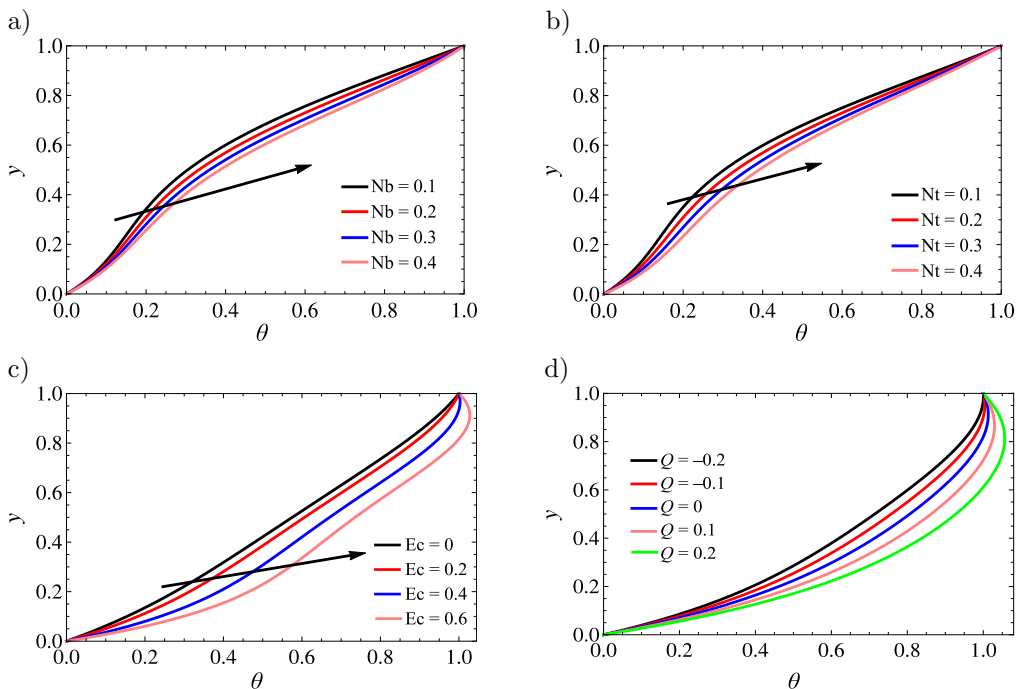


FIG. 4. Temperature distributions; impacts of: a) Nb, b) Nt, c) Ec, d) Q .

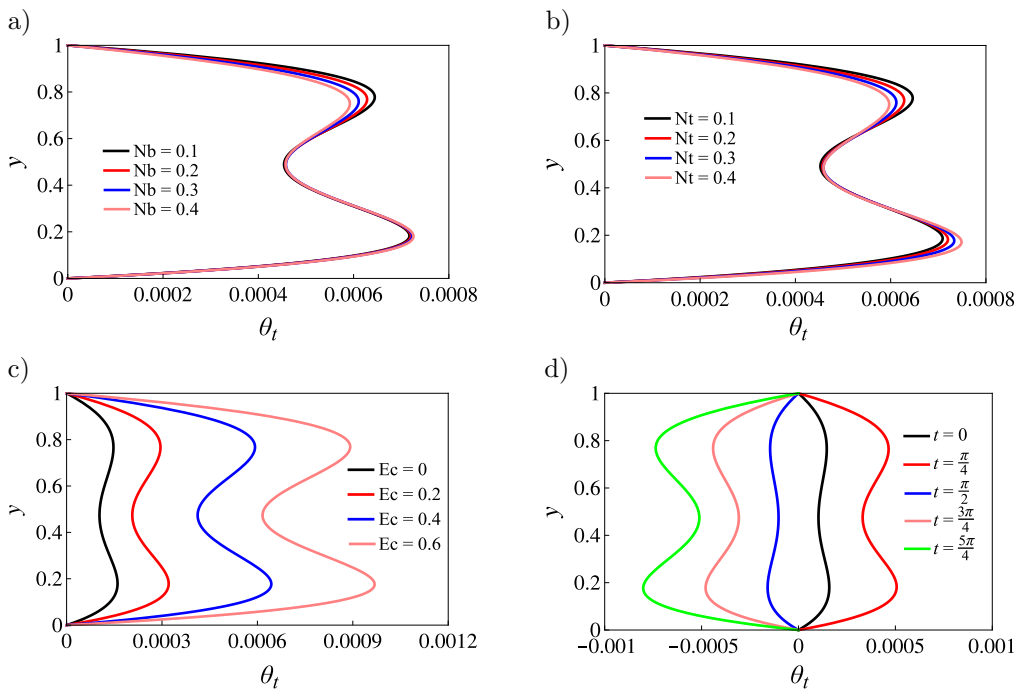


FIG. 5. Unsteady temperature distributions; impacts of: a) Nb, b) Nt, c) Ec, d) t .

in unsteady temperature distributions for different values of Nb , Nt , and Ec . Notably, it is observed that the unsteady temperature fluctuates with rising Nb , Nt , and Ec , with the maximum occurring closer to the walls. The impact of t on the unsteady temperature profile is exhibited in Fig. 5d. The unstable temperature profiles are observed to oscillate as t increases.

The distribution of nanoparticle concentration is shown in Fig. 6 for different values of Nb , Nt , Le , and γ . When Nb increases, the concentration of nanoparticles decreases, as shown in Fig. 6a. Conversely, when Nt increases, the concentration gradually increases (Fig. 6b). Figure 6c illustrates the decrease in nanoparticle concentration due to higher values of the Lewis number. Figure 6d depicts the influence of concentration distribution. It is observed that the distributions of nanoparticle concentrations decrease with an increase of destructive chemical reaction ($\gamma > 0$). This is due to fact that increasing destructive chemical reaction leads to a decrease in the concentration boundary layer because the destructive chemical reaction reduces the solutal boundary layer thickness and increases the mass transfer.

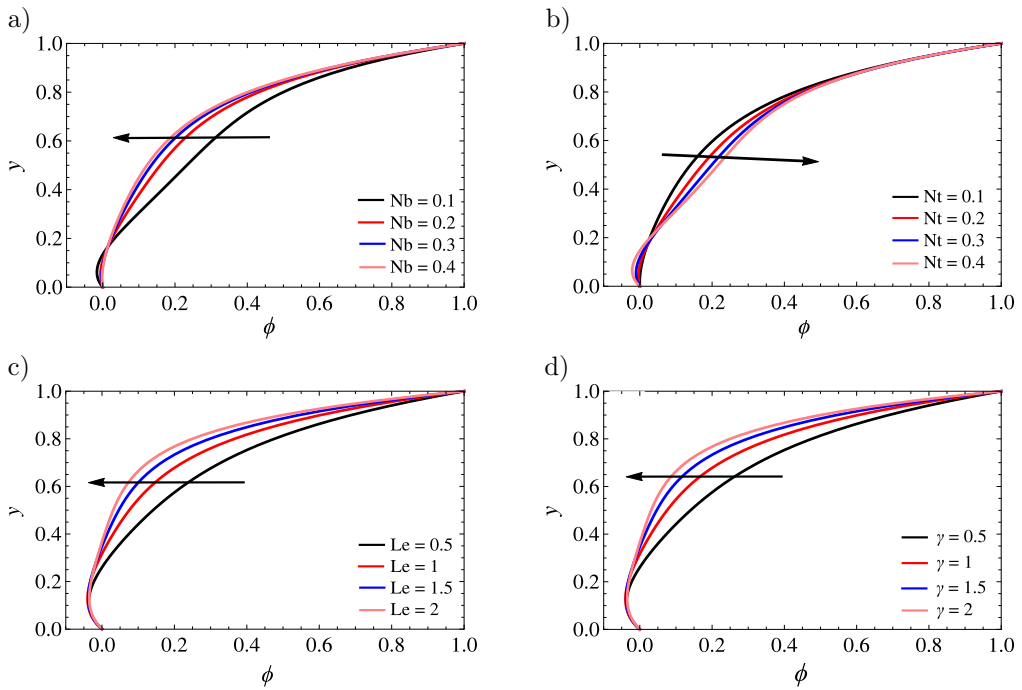


FIG. 6. Nanoparticle concentration distributions; impacts of: a) Nb , b) Nt , c) Le , d) γ .

The impacts of Nb , Nt , Le , and γ on ϕ_t are shown in Fig. 7. Figure 7 describes the variation in unsteady nanoparticle concentration distribution for various values of Nb , Nt , Le , and γ . One can notice that the unsteady nanopar-

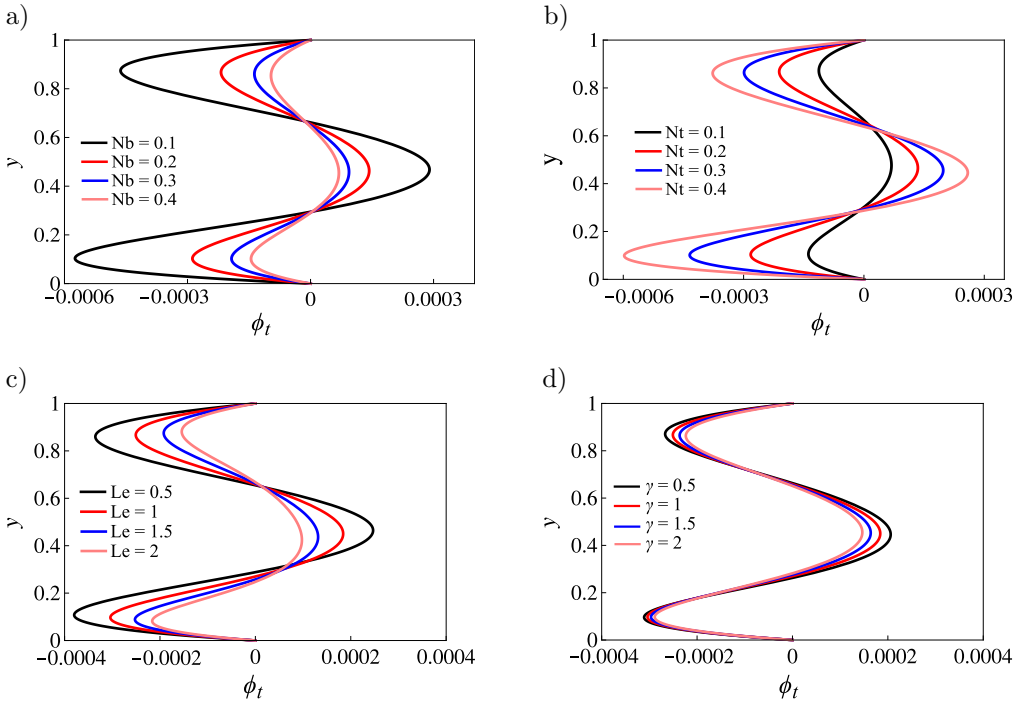


FIG. 7. Unsteady nanoparticle concentration distributions; impacts of: a) Nb , b) Nt , c) Le , d) γ .

ticle concentration fluctuates with rising Nb , Nt , Le , and γ and the maximum concentration is located closer to the walls. Figure 8 depicts the impact of k_0 and M on the mass flux distribution (Q_1) against H . As seen in Fig. 8a, Q_1 decreases for a given rise in the Powell-Eyring fluid parameter. By changing M , the opposite pattern can be observed (see Fig. 8b). To confirm the accuracy of the existing model, Fig. 9 presents a comparative study between a numerical method and the findings generated by an analytical approach (perturbation)

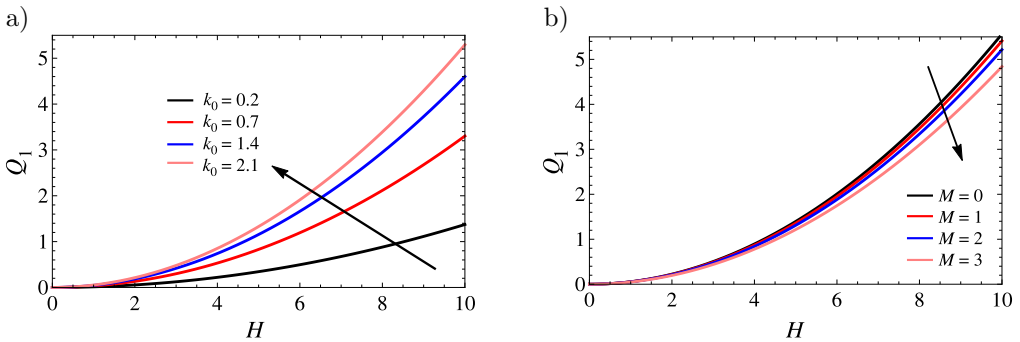


FIG. 8. Mass flux distributions; impacts of: a) k_0 , b) M .

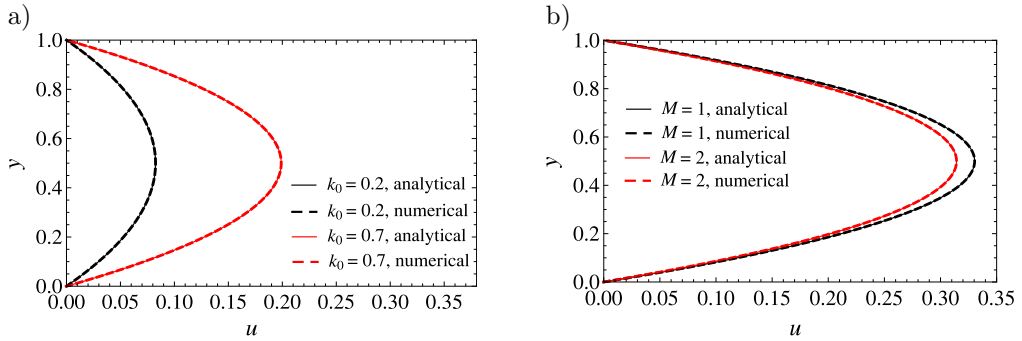


FIG. 9. Comparative study between numerical and analytical studies on velocity distributions; impacts of: a) k_0 , b) M .

for velocity distribution. The changes of Sh and Nu for different values of k_0 , Nt , Nb , and Le are shown in Table 1. In this case, the bottom and top walls' respective Sherwood and Nusselt numbers are denoted by the symbols Sh_0 , Sh_1 and Nu_0 , Nu_1 , respectively. Interestingly, Nu increases at the channel's upper boundary while decreasing at the lower boundary when the Powell-Eyring fluid parameter increases. For the Brownian motion parameter, the behaviour is the opposite. At the bottom and top walls, one can see that the Nusselt number is

Table 1. Variations of Nu and Sh for different values of k_0 , Nb , Nt , and Le .

Parameter	Values	Nu		Sh	
		Nu_0	Nu_1	Sh_0	Sh_1
k_0	0.2	0.1823	1.3324	-1.3465	4.7949
	0.7	0.1246	1.8973	-1.7483	5.2897
	1.4	0.1107	2.3451	-2.0642	6.1821
	2.1	0.1040	2.9960	-2.3247	6.3411
Nb	0.15	3.4432	-1.2649	-2.0065	6.3704
	0.20	3.6989	-1.3981	-1.8347	6.0815
	0.30	4.5901	-1.4843	-1.3102	5.7634
	0.40	5.0769	-1.5182	-1.2873	5.4988
Nt	0.1	2.2207	0.1389	-0.2767	-0.0419
	0.2	3.6991	0.1587	-1.5984	-0.0845
	0.3	5.6461	0.1725	-4.7136	-0.1618
	0.4	5.9985	0.1993	-5.8071	-0.2007
Le	0.5	3.7471	0.0844	-0.1277	1.8440
	1.0	3.6877	0.0660	-0.5417	2.6507
	1.5	3.6043	0.0604	-1.2661	2.7859
	2.0	3.5520	0.0573	-2.5322	3.0254

a rising function of Nt . For the Lewis number, the behaviour is the exact reverse. The same table shows that while the Powell-Eyring fluid parameter and Lewis number increase near the top wall, they drop at the bottom wall. For the Brownian motion parameter, the behaviour is the opposite. One can observe that at the lower and upper boundaries of the channel Sherwood number decreases with Nt .

5. CONCLUSIONS

The pulsatory flow of Powell-Eyring nanofluid using Buongiorno's model in a horizontal channel was investigated numerically, accounting for the impacts of thermophoresis and Brownian motion. This investigation holds significance in the field of food processing system, pressure surges (pulsatile flow application), biomedical engineering, and cancer therapeutics. Our analysis demonstrates that an inclined magnetic field, chemical reaction, and thermal radiation affect the flow. The governing partial differential equations were transformed into a system of ordinary differential equations by employing the perturbation method, then solved by adopting the fourth-order Runge-Kutta method along with the aid of the shooting technique. The velocity increases with a rise in the Eyring-Powell nanofluid parameter and frequency parameter, whereas a rise in the inclination angle decreases the velocity. Due to the effects of periodic pressure gradient, the fluid's unsteady velocity and temperature fluctuate over time. Moreover, as the parameters of the chemical reaction and Lewis number increase, the nanoparticle concentration distribution decreases.

APPENDIX

$$m_{1,2} = \frac{\pm \sqrt{4(1+k_0)M^2 \sin^2 \alpha}}{2(1+k_0)},$$

$$A_3 = \frac{H^2}{M^2 \sin^2 \alpha},$$

$$A_1 = \frac{A_3(e^{m_1} - 1)}{(e^{m_1} - e^{m_2})} - A_3,$$

$$A_2 = -\frac{A_3(e^{m_1} - 1)}{(e^{m_1} - e^{m_2})},$$

$$m_{3,4} = \frac{\pm \sqrt{4(1+k_0)(M^2 \sin^2 \alpha + iH^2)}}{2(1+k_0)},$$

$$A_6 = \frac{H^2}{(M^2 \sin^2 \alpha + iH^2)},$$

$$A_5 = -\frac{A_6(e^{m_3} - 1)}{(e^{m_3} - e^{m_4})},$$

$$A_4 = \frac{A_6(e^{m_3} - 1)}{(e^{m_3} - e^{m_4})} - A_6,$$

$$m_{5,6} = \frac{\pm \sqrt{4(1 + k_0)(M^2 \sin^2 \alpha + 2iH^2)}}{2(1 + k_0)},$$

$$A_7 = 0,$$

$$A_8 = 0.$$

REFERENCES

1. CHOI S.U.S., Enhancing thermal conductivity of fluids with nanoparticles, [in:] *Proceedings of the 1995 ASME International Mechanical Engineering Congress and Exposition, San Francisco, USA (ASME, FED 231/MD)*, **66**: 99–105, 1995, <https://cir.nii.ac.jp/crid/1571980074227838464>.
2. KUMAR B., SRINIVAS S., Unsteady hydromagnetic flow of Eyring-Powell nanofluid over an inclined permeable stretching sheet with Joule heating and thermal radiation, *Journal of Applied and Computational Mechanics*, **6**(2): 259–270, 2019, doi: 10.22055/jacm.2019.29520.1608.
3. WAQAS H., NAEEM H., MANZOOR U., SIVASANKARAN S., ALHARBI A.A., ALSHOMRANI A.S., MUHAMMAD T., Impact of electro-magneto-hydrodynamics in radiative flow of nanofluids between two rotating plates, *Alexandria Engineering Journal*, **61** (12): 10307–10317, 2022, doi: 10.1016/j.aej.2022.03.059.
4. ALSAEDI A., HAYAT T., QAYYUM S., YAQOOB R., Eyring-Powell nanofluid flow with non-linear mixed convection: Entropy generation minimization, *Computer Methods and Programs in Biomedicine*, **186**: 105183, 2020, doi: 10.1016/j.cmpb.2019.105183.
5. BUONGIORNO J., Convective transport in nanofluids, *Journal of Heat Transfer*, **128** (3): 240–250, 2006, doi: 10.1115/1.2150834.
6. HAYAT T., SAJJAD R., MUHAMMAD T., ALSAEDI A., ELLAHI R., On MHD nonlinear stretching flow of Powell-Eyring nanomaterial, *Results in Physics*, **7**: 535–543, 2017, doi: 10.1016/j.rinp.2016.12.039.
7. KUMAR C.K., SRINIVAS S., REDDY A.S., MHD pulsating flow of Casson nanofluid in a vertical porous space with thermal radiation and Joule heating, *Journal of Mechanics*, **36**(4): 535–549, 2020, doi: 10.1017/jmech.2020.5.
8. MALLICK B., MISRA J.C., Peristaltic flow of Eyring-Powell nanofluid under the action of an electromagnetic field, *Engineering Science and Technology, an International Journal*, **22**(1): 266–281, 2019, doi: 10.1016/j.jestch.2018.12.001.

9. SHEIKHOESLAMI M., CHAMKHA A.J., RANA P., MORADI R., Combined thermophoresis and Brownian motion effects on nanofluid free convection heat transfer in an L-shaped enclosure, *Chinese Journal of Physics*, **55**(6): 2356–2370, 2017, doi: 10.1016/j.cjph.2017.09.011.
10. SHEHZAD N., ZEESHAN A., ELLAHI R., VAFAI K., Convective heat transfer of nanofluid in a wavy channel: Buongiorno's mathematical model, *Journal of Molecular Liquids*, **222**: 446–455, 2016, doi: 10.1016/j.molliq.2016.07.052.
11. HAYAT T., SHAFIQ A., ALSAEDI A., ASGHAR S., Effect of inclined magnetic field in flow of third grade fluid with variable thermal conductivity, *AIP Advances*, **5**: 087108, 2015, doi: 10.1063/1.4928321.
12. KUMAR C.K., SRINIVAS S., Simultaneous effects of thermal radiation and chemical reaction on hydromagnetic pulsatile flow of a Casson fluid in a porous space, *Engineering Transactions*, **65**(3): 461–481, 2017.
13. ACHARYA N., MAITY S., KUNDU P.K., Influence of inclined magnetic field on the flow of condensed nanomaterial over a slippery surface: the hybrid visualization, *Applied Nanoscience*, **10**: 633–647, 2020. doi: 10.1007/s13204-019-01123-0.
14. KHAN A.A., NAEEM S., ELLAHI R., SAIT S.M., VAFAI K., Dufour and Soret effects on Darcy–Forchheimer flow of second-grade fluid with the variable magnetic field and thermal conductivity, *International Journal of Numerical Methods for Heat & Fluid Flow*, **30**(9): 4331–4347, 2020, doi: 10.1108/HFF-11-2019-0837.
15. AHMED S.E., ELSHEHABEY H.M., OZTOP H.F., Natural convection of three-dimensional non-Newtonian nanofluids with Marangoni effects and inclined magnetic fields, *International Communications in Heat and Mass Transfer*, **137**: 106288, 2022, doi: 10.1016/j.icheatmasstransfer.2022.106288.
16. KALADHAR K., REDDY K.M., SRINIVASACHARYA D., Inclined magnetic field, thermal radiation, and Hall current effects on mixed convection flow between vertical parallel plates, *Journal of Heat Transfer*, **141**(10): 102501, 2019, doi: 10.1115/1.4044391.
17. NATH R., MURUGESAN K., Impact of nanoparticle shape on thermo-solutal buoyancy induced lid-driven-cavity with inclined magnetic-field, *Propulsion and Power Research*, **11**(1): 97–117, 2022, doi: 10.1016/j.jprr.2022.01.002.
18. NOREEN S., QASIM M., Peristaltic flow with inclined magnetic field and convective boundary conditions, *Applied Bionics and Biomechanics*, **11** (1–2): 61–67, 2014, doi: 10.1155/2014/426217.
19. BIANCO V., TRUBATCH A.D., WEI H., YECKO P., Quantifying volume loss of a magnetically localized ferrofluid bolus in pulsatile pipe flow, *Journal of Magnetism and Magnetic Materials*, **524**: 167595, 2021, doi: 10.1016/j.jmmm.2020.167595.
20. CHENG Z., JELLY T.O., ILLINGWORTH S.J., MARUSIC I., OOI A.S.H., Forcing frequency effects on turbulence dynamics in pulsatile pipe flow, *International Journal of Heat and Fluid Flow*, **82**: 108538, 2020, doi: 10.1016/j.ijheatfluidflow.2020.108538.
21. GOVINDARAJULU K., REDDY A.S., Magneto-hydrodynamic pulsatile flow of third grade hybrid nanofluid in a porous channel with Ohmic heating and thermal radiation effects, *Physics of Fluids*, **34**: 013105, 2022, doi: 10.1063/5.0074894.
22. RADHAKRISHNAMACHARYA G., MAITI M.K., Heat transfer to pulsatile flow in a porous channel, *International Journal of Heat and Mass Transfer*, **20**(2): 171–173, 1977, doi: 10.1016/0017-9310(77)90009-6.

23. SRINIVAS S., KUMAR C.K., REDDY A.S., Pulsating flow of Casson fluid in a porous channel with thermal radiation, chemical reaction and applied magnetic field, *Nonlinear Analysis: Modelling and Control*, **23**(2): 213–233, 2018, doi: 10.15388/NA.2018.2.5.
24. WANG C.-Y., Pulsatile flow in a porous channel, *Journal of Applied Mechanics*, **38**(2): 553–555, 1971, doi: 10.1115/1.3408822.
25. DATTA N., DALAL D.C., MISHRA S.K., Unsteady heat transfer to pulsatile flow of a dusty viscous incompressible fluid in a channel, *International Journal of Heat and Mass Transfer*, **36**(7): 1783–1788, 1993, doi: 10.1016/S0017-9310(05)80164-4.
26. HORNG T.-L., LIN W.-L., LIAUH C.-T., SHIH T.-C., Effects of pulsatile blood flow in large vessels on thermal dose distribution during thermal therapy, *Medical Physics*, **34**(4): 1312–1320, 2007, doi: 10.1118/1.2712415.
27. KUMAR C.K., SRINIVAS S., Pulsating hydromagnetic flow of Casson fluid in a vertical channel filled with non-Darcian porous medium, *Heat Transfer*, **50**(6): 5225–5239, 2021, doi: 10.1002/htj.22121.
28. SANKAR D.S., A two-fluid model for pulsatile flow in catheterized blood vessels, *International Journal of Non-Linear Mechanics*, **44**(4): 337–351, 2009, doi: 10.1016/j.ijnonlinmec.2008.12.008.
29. SHAWKY H.M., Pulsatile flow with heat transfer of dusty magnetohydrodynamic Re-Eyring fluid through a channel, *Heat Mass Transfer*, **45**: 1261–1269, 2009, doi: 10.1007/s00231-009-0502-0.
30. SRINIVAS S., KUMAR C.K., REDDY A.S., Dufour and Soret effects on pulsatile hydromagnetic flow of Casson fluid in a vertical non-Darcian porous space, *Nonlinear Analysis: Modelling and Control*, **27**(4): 669–683, 2022, doi: 10.15388/namc.2022.27.26678.
31. THAMIZHARASAN T., REDDY A.S., Pulsating hydromagnetic flow of Au-blood Jeffrey nanofluid in a channel with Joule heating and viscous dissipation, *Nanoscience and Technology: An International Journal*, **13**(2): 1–13, 2022, doi: 10.1615/NanoSciTechnolIntJ.2022039247.
32. WANG X., QIAO Y., QI H., XU H., Numerical study of pulsatile non-Newtonian blood flow and heat transfer in small vessels under a magnetic field, *International Communications in Heat and Mass Transfer*, **133**: 105930, 2022, doi: 10.1016/j.icheatmasstransfer.2022.105930.

Received November 12, 2022; accepted version June 19, 2023.



Copyright © 2023 The Author(s).

This is an open-access article distributed under the terms of the Creative Commons Attribution-ShareAlike 4.0 International (CC BY-SA 4.0 <https://creativecommons.org/licenses/by-sa/4.0/>) which permits use, distribution, and reproduction in any medium, provided that the article is properly cited. In any case of remix, adapt, or build upon the material, the modified material must be licensed under identical terms.